

# A Novel Characterization of the Population Area Under the Risk Coverage Curve (AURC) and Rates of Finite Sample Estimators

Han Zhou<sup>1</sup>      Jordy Van Landeghem<sup>2</sup>    Teodora Popordanoska<sup>1</sup>    Matthew B. Blaschko<sup>1</sup>  
<sup>1</sup>KU Leuven, Belgium      <sup>2</sup>Instabase, San Francisco, USA

## Abstract

The selective classifier (SC) has garnered increasing interest in areas such as medical diagnostics, autonomous driving, and the justice system. The Area Under the Risk-Coverage Curve (AURC) has emerged as the foremost evaluation metric for assessing the performance of SC systems. In this work, we introduce a more straightforward representation of the population AURC, interpretable as a weighted risk function, and propose a Monte Carlo plug-in estimator applicable to finite sample scenarios. We demonstrate that our estimator is consistent and offers a low-bias estimation of the actual weights, with a tightly bounded mean squared error (MSE). We empirically show the effectiveness of this estimator on a comprehensive benchmark across multiple datasets, model architectures, and Confidence Score Functions (CSFs).

*risk*—while maximizing *coverage*, ensuring the model provides accurate predictions for as many instances as possible. This dual focus on selective risk and coverage motivates the development and evaluation of SC systems.

Prominent evaluation metrics in SC systems include the risk coverage curve (RC) (El-Yaniv et al., 2010), the area under the risk-coverage curve (AURC) (Geifman et al., 2018), and the normalized AURC (E-AURC) (Moon et al., 2020). These metrics, predicated on selective risk and coverage, may present challenges in interpretation, particularly in the context of finite sample datasets. A few studies (Geifman et al., 2018; Franc et al., 2023) have explored approximations for AURC in such scenarios. For instance, Franc et al. (2023) gave another expression of the empirical AURC, defining it as the arithmetic mean of empirical selective risks across evenly distributed coverage intervals  $[0, 1]$  with step  $\frac{1}{n}$ . However, most existing works typically use their estimator as substitutes for population AURC, without accounting for potential biases or variances in these estimators.

Inspired by these findings, we propose a more intuitive asymptotic formulation for the population AURC and introduce a Monte Carlo-based plug-in estimator that comes with theoretical support. This asymptotic formulation is explicitly defined as a reweighted risk function. Additionally, the Monte Carlo estimator is characterized as a linear weighted sum of empirical risks, with weights determined solely by empirical rankings within the sample. We also analyze the statistical characteristics of this weight estimator, including its MSE and bias. Finally, we illustrate the efficacy of the proposed estimator through both evaluation and fine-tuning tasks, spanning various model architectures, CSFs, and datasets.

## 1 INTRODUCTION

In safety-critical scenarios such as autonomous driving, medical diagnostics, and the justice system (Leibig et al., 2022; Dvijotham et al., 2023; Groh et al., 2024; Berk et al., 2021), selective classifiers (SC) are paramount for their ability to withhold predictions under conditions of uncertainty, thereby mitigating associated risks and enhancing the reliability of the models. Specifically, these classifiers employ cost-based models (Chow, 1970) with a reject region to balance the risks of wrong predictions against the non-decision costs. The goal of an effective SC system is to minimize the expected misclassification costs—termed *selective*

## 2 RELATED WORK

**Evaluation Metrics:** The Area Under the Risk Coverage curve (AURC) and its normalized counterpart Excess-AURC (E-AURC) (Geifman et al., 2018) are

Correspondence to han.zhou@esat.kuleuven.be.

<sup>2</sup>Work was done at KU Leuven prior to joining Instabase. Preprint. Under review.

the most prevalent evaluation metrics for SC systems that compute the risk or the error with accepted predictions at different confidence thresholds. Furthermore, Geifman et al. (2018) gave an estimation of AURC in terms of the 0/1 loss (accuracy). Additionally, Cattelan and Silva (2023a) have proposed a min-max scaled version of E-AURC, designed to maintain a monotonous relationship with AURC, thereby enhancing its consistency in performance assessment. Franc et al. (2023) have introduced a Fisher consistency estimator, the SELE score, which serves as a lower bound for the AURC. Conversely, Traub et al. (2024) argues that these metrics related to the selective risk, which only focus on the risk w.r.t accepted predictions, do not suffice for a holistic assessment. To address this limitation, they developed the Area under the Generalized Risk Coverage curve (AUGRC), which quantifies the average risk of undetected failures across all predictions, thereby providing a more holistic measure of system reliability. However, most studies directly employ their estimators as proxies for population AURC, even in finite sample scenarios, without adequately investigating the effectiveness of these estimators in such cases. In contrast to prior studies, this work concentrates on estimating the population AURC in the context of finite samples. We aim to introduce an effective estimator with a theoretical guarantee and conduct an empirical analysis, comparing it with existing AURC estimators.

**Uncertainty estimation:** There has been a large number of works (Geifman et al., 2018; Abdar et al., 2021; Zhu et al., 2023) that highlight the importance of confidence scoring and uncertainty quantification associated with predictions. In practice<sup>1</sup>, commonly used CSFs fall into two main categories: ensemble approaches and post-hoc methods. Ensemble methods (Lakshminarayanan et al., 2017; Teye et al., 2018; Liu et al., 2023; Xia and Bouganis, 2023; Hou et al., 2023) require multiple forward passes to approximate the posterior predictive distribution, exemplified by the Monte-Carlo Dropout (MCD) techniques (Gal and Ghahramani, 2016). However, recent works (Cattelan and Silva, 2023a; Xia and Bouganis, 2022) suggest that the ensemble may not be crucial for enhancing uncertainty estimation but rather serves to improve the predictions through a set of diverse classifiers. Thus such methods are not considered further in this paper. In contrast, post-hoc estimators leverage the logits produced by the model to evaluate its performance. Popular methods include *Maximum Softmax Probability* (MSP) (Hendrycks and Gimpel, 2016), *Maximum Logit Score* (MaxLogit) (Hendrycks et al., 2019), *Soft-*

*max Margin* (Belghazi and Lopez-Paz, 2021), *Negative Entropy* (Liu et al., 2020). Furthermore, Cattelan and Silva (2023b) shows that the maximum  $p$ -norm of the logits (MaxLogit- $p$ Norm) can work better than MSP in uncertainty estimation when dealing with some models. Specifically, normalizing the logits with  $\ell_2$  norm has been shown to yield more distinct confidence scores, as evidenced in Wei et al. (2022). Gomes et al. (2022) propose the *Negative Gini Score* that utilizes the squared  $\ell_2$  norm of the softmax probability. In this study, we examine the impact of the post-hoc CSFs on the AURC, aiming to offer a thorough evaluation of AURC approximation.

### 3 PERFORMANCE EVALUATION OF SELECTIVE CLASSIFIER

#### 3.1 Problem setting

Let  $\mathcal{X} \subseteq \mathbb{R}^d$  be the input space,  $\mathcal{Y} \subseteq \{0, 1\}^k$  be the label space, and  $P(x, y)$  be the unknown joint distribution over  $\mathcal{X} \times \mathcal{Y}$ . We consider a classifier  $f : \mathcal{X} \rightarrow \mathcal{Y}$  and a *confidence scoring function* (CSF)  $g : \mathcal{X} \rightarrow [0, 1]$ , the selective classification system  $(f, g)$  at an input  $x$  can then be described by

$$(f, g)(x) := \begin{cases} f(x) & \text{if } g(x) \geq \tau(x), \\ \text{"abstain"} & \text{otherwise.} \end{cases} \quad (1)$$

where "abstain" is triggered when  $g(x)$  falls below a decision threshold  $\tau(x) \in \mathbb{R}$ . Given a loss function  $\ell : \mathcal{Y} \times \mathcal{Y} \rightarrow \mathbb{R}$ , the true risk of  $f$  w.r.t.  $P(x, y)$  is  $R(f) = \mathbb{E}_{P(x, y)}[\ell(f(x), y)]$ . Given the finite sample dataset  $D_n = \{(x_i, y_i)\}_{i=1}^n \subseteq (\mathcal{X} \times \mathcal{Y})$  sampled i.i.d. from  $P(x, y)$ , the true risk can be inferred from the *empirical risk*  $\hat{r}(f) := \frac{1}{n} \sum_{i=1}^n \ell(f(x_i), y_i)$ . For practical purposes, we define the selection function  $\tilde{g}$  as  $\tilde{g}(x) = \mathbb{I}[g(x) \geq \tau(x)]$ . The form of the decision threshold function  $\tau(x)$  varies based on the specific scenario and the evaluation metric being used. It can either be a pre-defined constant i.e.  $\tau(x) = c$  for all  $x \in \mathcal{X}$ , or it may be a function that adapts based on the predicted uncertainty of observations.

#### 3.2 Evaluation Metrics

One common way to assess the performance of selective classifiers is the risk-coverage curve (RC curve) (El-Yaniv et al., 2010), where *coverage* measures the probability mass of the input space that is not rejected in Eq. (1), denoted by  $\mathbb{E}_{P(x)}[\tilde{g}(x)]$ . And the selective risk w.r.t.  $P(x, y)$  is then defined as

$$R(f, \tilde{g}) := \frac{\mathbb{E}_{P(x, y)}[\ell(f(x), y)\tilde{g}(x)]}{\mathbb{E}_{P(x)}[\tilde{g}(x)]}. \quad (2)$$

<sup>1</sup>While it is preferable for the output domain of CSFs to be in  $[0, 1]$  for easier determination of selection thresholds, this is not a strict requirement.

$\ell$  is typically the 0/1 error, making  $R(f, \tilde{g})$  the selective error. As indicated by the equation above, risk and coverage are strongly dependent, where rejecting more examples reduces selective risk but also results in lower coverage. Nevertheless, this metric considers the rejection threshold  $\tau(\cdot)$  as a fixed constant, which may be appropriate in contexts such as medical diagnostics, where the cost of erroneous predictions can be consistently quantified across all instances, irrespective of the broader characteristics of the population. However, such an approach may not be suitable in domains like credit scoring, where predictions serve to estimate the probability of debt repayment. In such contexts, withholding predictions when the uncertainty surpasses a predetermined threshold (e.g., 10%) may be less appropriate, as it uniformly disregards applicants without accounting for their distinct risk profiles or the comparative risk distribution across the entire applicant pool. Another notable consideration regarding evaluation metrics is that accuracy is often an insufficient measure for classification performance in various real-world contexts, particularly in the presence of class imbalance problem or in tasks requiring pixel-level classification. Consequently, the evaluation metric should be adaptable to accommodate different loss functions, ensuring a more comprehensive assessment of model performance under diverse conditions.

### 3.2.1 A Plug-In Estimator of AURC

Driven by the aforementioned considerations, Geifman et al. (2018) introduced the AURC metric, designed to offer a robust evaluation framework for classifiers by effectively capturing performance across varying rejection thresholds that are determined based on the distribution of samples within the population. Specifically, given a CSF  $g(x)$ , then the population AURC is generally defined as

$$\text{AURC}_p(f) = \mathbb{E}_{x \sim P(x)} \frac{\mathbb{E}_{(\tilde{x}, \tilde{y}) \sim P(x, y)} \ell(f(\tilde{x}), \tilde{y}) \mathbb{I}[g(\tilde{x}) \geq g(x)]}{\mathbb{E}_{\tilde{x} \sim P(x)} \mathbb{I}[g(\tilde{x}) \geq g(x)]} \quad (3)$$

Given a finite sample of size  $n$ , namely  $D_n = \{(x_i, y_i)\}_{i=1}^n \subseteq (\mathcal{X} \times \mathcal{Y})$ , which is sampled i.i.d. from a joint probability distribution  $P(x, y)$ , then the finite sample estimator of population AURC is given by

$$\widehat{\text{AURC}}_p(f) = \frac{1}{n} \sum_{j=1}^n \frac{\frac{1}{n} \sum_{i=1}^n \ell(f(x_i), y_i) \mathbb{I}[g(x_i) \geq g(x_j)]}{\frac{1}{n} \sum_{i=1}^n \mathbb{I}[g(x_i) \geq g(x_j)]} \quad (4)$$

$$= \sum_{i=1}^n \hat{\alpha}_i \ell(f(x_i), y_i) \quad (5)$$

where  $\hat{\alpha}_i = \frac{1}{n} \sum_{j=1}^{r_i} \frac{1}{n-j+1}$ . Clearly, this weight estimator is an unbiased estimator of the true weight for population AURC. The second equation can be derived when our data is sorted in ascending order

according to the CSF. The computation cost of this metric is  $\mathcal{O}(n \log(n))$ , primarily due to the sorting operation on our data. Let us denote  $r_i$  as the rank of  $x_i$  and  $H_n$  is the  $n$ th harmonic number given by  $H_n := \sum_{k=1}^n \frac{1}{k}$ . From the plug-in estimator in Eq. (5), the empirical AURC can be interpreted as a weighted sum of the empirical risk. Each individual loss is weighted by  $\hat{\alpha}_i$  which accounts for the importance of this point. Since the  $n$ th harmonic number is given by  $H_n := \sum_{k=1}^n \frac{1}{k}$ , it can also be expressed in terms of the digamma function  $\psi(n) := \frac{\Gamma'(n)}{\Gamma(n)}$  such that  $H_n = \psi(n+1) + \gamma$  where  $\gamma \approx 0.577$  is the Euler–Mascheroni constant. Defining  $H_0 = 0$ , we can write the weight in terms of harmonic numbers or digamma functions

$$\hat{\alpha}_i = \frac{1}{n} (H_n - H_{n-r_i}) = \frac{1}{n} (\psi(n+1) - \psi(n-r_i+1)). \quad (6)$$

Franc et al. (2023) gave another expression of the empirical AURC in Eq. (4) that can be interpreted as an arithmetic mean of the empirical selective risks corresponding to the coverage spread evenly over the interval  $[0, 1]$  with step  $\frac{1}{n}$ . In addition, they proposed a coarse lower bound, referred to as the SELE score given by

$$\Delta_{\text{sele}}(f) = \frac{1}{n^2} \sum_{i=1}^n \sum_{j=1}^n \ell(f(x_i), y_i) \mathbb{I}[g(x_i) \geq g(x_j)], \quad (7)$$

as an alternative to the AURC. They also prove  $2\Delta_{\text{sele}}(f)$  is a tight upper bound to AURC. Given the sorted data according to CSF, we can rewrite it as

$$\Delta_{\text{sele}}(f) = \sum_{i=1}^n \frac{r_i}{n^2} \ell(f(x_i), y_i) \quad (8)$$

where  $r_i$  is the rank within the finite sample. However, this estimator still relies on sorting operations and its bias cannot be ignored compared with Eq. (5). In this paper, we will give a more straightforward definition of population AURC, propose a finite sample estimator for it, and subsequently conduct a comparative analysis against the SELE score in Section 4.

### 3.2.2 Asymptotics of $\text{AURC}_p$

In order to better understand the population AURC, we study the asymptotic behavior and consistency of the plug-in AURC estimator.

**Proposition 1** (Asymptotic consistency). *Define  $\beta_i$  as the rank percentile of the observation  $(x_i, y_i)$  ranked by CSF such that  $\beta_i = \frac{r_i}{n} \in (0, 1)$ . Under this definition, the parameter  $n\alpha_i$  is consistent, converging to the limit*

$$\lim_{n \rightarrow \infty} n\hat{\alpha}_i = -\ln(1 - \beta_i).$$

*Proof.* Define  $\beta_i = \frac{r_i}{n} \in (0, 1)$  and take the limit

$$\begin{aligned} \lim_{n \rightarrow \infty} [H_n - H_{n-\beta_i n}] &= \lim_{n \rightarrow \infty} [\psi(n+1) - \psi(n - \beta_i n + 1)] \\ &= \lim_{n \rightarrow \infty} \left[ \ln(n+1) - \frac{1}{2(n+1)} - \ln(n - \beta_i n + 1) + \frac{1}{2(n - \beta_i n + 1)} \right] \\ &= \lim_{n \rightarrow \infty} \left[ -\frac{1}{2(n+1)} + \frac{1}{2(n - \beta_i n + 1)} - \ln\left(1 - \beta_i + \frac{\beta_i}{n+1}\right) \right] \\ &= -\ln(1 - \beta_i) \end{aligned} \quad (9)$$

where the 2nd equation was obtained using the asymptotic result that  $\psi(n) \rightarrow \ln n - \frac{1}{2n}$  as  $n \rightarrow \infty$ .  $\square$

In the limit of infinite data, we notice that

$$\lim_{n \rightarrow \infty} \sum_{i=1}^n \hat{\alpha}_i = \int_0^1 -\ln(1-z) dz = 1 \quad (10)$$

for  $\beta_i \in (0, 1)$ , indicating that in this case, the sum over  $\hat{\alpha}_i$  calculated through Eq. (6) will converge to 1. This directly demonstrates that  $\text{AURC}_p$  is a redistribution of the risk function. Inspired by this fact and Prop 1, we propose the following asymptotic formulation that can be considered equivalent to the population AURC in Eq. (3).

**Definition 2** (Asymptotic equivalence to  $\text{AURC}_p$ ). Define function  $G(x)$  as the CDF of the random variable  $g(x)$

$$G(x) = \Pr(g(\tilde{x}) \leq g(x)) = \int \mathbb{I}[g(\tilde{x}) \leq g(x)] dP(\tilde{x}) \quad (11)$$

then population AURC in Eq. (3) is asymptotically equivalent to the following expression:

$$\text{AURC}_a(f) = \int -\ell(f(x), y) \ln(1 - G(x)) dP(x, y). \quad (12)$$

In the context of infinite data, the cumulative distribution score can be computed directly from the population, which leads to the plug-in coefficient in Eq. (12)

$$\alpha_i^* = -\frac{1}{n} \ln(1 - G(x_i)). \quad (13)$$

Since  $\{G(x_i)\}$  behave as i.i.d. samples from a uniform distribution when  $x_i$  are themselves i.i.d. from  $P(x)$ , the summation  $\lim_{n \rightarrow \infty} \sum_{i=1}^n \alpha_i^*$  will also converge to one. Compared to  $\text{AURC}_p$  in Eq. 3, this asymptotic expression is directly formulated as a reweighted risk function where the weights are detailed in Eq. (13). In practice, when dealing with only a finite sample from the population, this cumulative distribution score is typically unknown to us. And it is straightforward to come up with an estimator for the weights in Eq. (12) that is

$$\tilde{\alpha}_i^* = -\frac{1}{n} \ln\left(1 - \frac{r_i}{n}\right) \quad (14)$$

with  $r_i$  as the rank within the sample. Obviously, this yields a consistent estimator and  $\lim_{n \rightarrow \infty} \sum_{i=1}^n \tilde{\alpha}_i^* = 1$ . However, the bias of this estimator may not be minimized, especially when the sample size is small. In the next section, we will explore an alternative estimator based on a kind of Monte Carlo integration, which exhibits reduced bias.

### 3.2.3 Monte Carlo estimator

First, we consider the simple case where we sample i.i.d.  $\{\beta_i\}_{1 \leq i \leq n} \sim \mathcal{U}[0, 1]$ , then sort this set in ascending order. Let  $r_i$  be the rank for  $\beta_i$  and set  $\alpha_i^* = -\ln(1 - \beta_i)$ . It is clear that we can find a lower variance estimate with the same bias by repeating the process and averaging the obtained  $\alpha_i^*$  estimates. The  $\beta_i$  are order statistics of the uniform distribution, and have known distribution (Jones, 2009, Section 2)

$$\beta_i \sim \text{Beta}(r_i, n + 1 - r_i) = \frac{\beta_i^{r_i-1} (1 - \beta_i)^{n-r_i}}{B(r_i, n + 1 - r_i)} \quad (15)$$

Consequently, the limit expectation of averaging our estimator with repeatedly resampled  $\beta_i$  will yield our finite sample estimator  $\hat{\alpha}_i^*$  given by

$$\hat{\alpha}_i^* = \frac{1}{n} \int_0^1 -\ln(1-x) \frac{x^{r_i-1} (1-x)^{n-r_i}}{B(r_i, n + 1 - r_i)} dx \quad (16)$$

$$= \frac{1}{n} (H_n - H_{n-r_i}) = \hat{\alpha}_i \quad (17)$$

which is exactly the same as Eq. (6). This low variance estimator of the weights also demonstrates that  $\text{AURC}_p$  and  $\text{AURC}_a$  can be equivalent in the infinite sample scenario.

For our population  $\text{AURC}_a$  in Eq. (12), we wish to estimate this quantity by the Monte Carlo integration. Since the cumulative distribution score  $G(x_i)$  is unknown, we need an estimator for Eq. (13). From the simple case, we can achieve this estimator by taking the conditional expectation

$$\mathbb{E} \left[ -\frac{1}{n} \ln(1 - G(x_i)) | \{g(x_j)\}_{1 \leq j \leq n} \right] = \underbrace{\frac{1}{n} (H_n - H_{n-r_i})}_{\hat{\alpha}_i^*} \quad (18)$$

where  $r_i$  is the rank of  $\{g(x_i)\}_{1 \leq i \leq n}$  when sorted in ascending order. This leads to the Monte Carlo plug-in estimator for  $\text{AURC}_a$ :

$$\widehat{\text{AURC}}_a(f) = \hat{\alpha}_i^* \ell(f(x_i), y_i) \quad (19)$$

for finite samples. The weights estimator  $\hat{\alpha}_i^*$  and losses are typically not independent as they both depend on the model's logits, making it difficult to derive the statistical properties of the above estimator. Therefore, we consider the properties of the weight estimator  $\hat{\alpha}_i^*$

based on the finite sample dataset. In the following Section, we will show that  $\hat{\alpha}_i^*$  is a biased estimator of  $\alpha_i^*$  and that the sum of the MSEs of these weight estimators is tightly bounded by  $\mathcal{O}\left(\frac{\ln(n)}{n^2}\right)$ .

For some specific data pair  $(x_i, y_i) \in (\mathcal{X}, \mathcal{Y})$  with unknown population rank percentile  $\beta_i$ , consider randomly sampling  $n - 1$  i.i.d. samples repeatedly from the population, and computing the expected  $\hat{\alpha}_i^*$  associated with  $(x_i, y_i)$ . For the procedure to be unbiased we require  $-\frac{1}{n} \ln(1 - \beta_i) - \mathbb{E}[\hat{\alpha}_i^* | G(x_i) = \beta_i] = 0$ . In fact, we have

$$\begin{aligned} & \mathbb{E}[\hat{\alpha}_i^* | G(x_i) = \beta_i] \\ &= \sum_{i=1}^n \frac{1}{n} (H_n - H_{n-r_i}) \Pr(r_i = i | G(x_i) = \beta_i) \end{aligned} \quad (20)$$

We notice that  $\Pr(r_i | G(x_i) = \beta_i)$  is a binomial distribution  $\text{Bin}(n - 1, \beta_i)$  and it can be written as follows:

$$\Pr(r_i = i | G(x_i) = \beta_i) = C_{i-1}^{n-1} \beta_i^{i-1} (1 - \beta_i)^{n-i} \quad (21)$$

because the probability of any i.i.d. sample being ranked below  $x_i$  is  $\beta_i$ , and there must be  $(i - 1)$  of them for the sample to be ranked  $i$ th, while the remaining  $(n - i)$  samples must be ranked higher, each with an independent probability of  $(1 - \beta_i)$ . Combining these results gives us:

$$\begin{aligned} \text{Bias}(\hat{\alpha}_i^* | G(x_i) = \beta_i) &= \mathbb{E}[\hat{\alpha}_i^* | G(x_i) = \beta_i] - \alpha_i^* \\ &= \frac{1}{n} \left( H_n - \sum_{i=1}^n H_{n-i} C_{i-1}^{n-1} \beta_i^{i-1} (1 - \beta_i)^{n-i} \right) - \alpha_i^*. \end{aligned} \quad (22)$$

This is not equal to zero in general, but is positive for smaller  $\beta_i$  and negative for larger  $\beta_i$ . The exact shape of the curve depends on the sample size  $n$  (Figure 1).

**Proposition 3 (MSE of  $\sum_{i=1}^n \hat{\alpha}_i^*$ ).** *The MSE of the sum of the weight estimators  $\hat{\alpha}_i^*$  is tightly bounded by  $\mathcal{O}\left(\frac{\ln(n)}{n^2}\right)$ .*

*Proof.* From asymptotic result in Prop.1, we calculate:

$$\begin{aligned} \text{MSE}(n\hat{\alpha}_i^*) &= \mathbb{E}_{\beta_i} [(n\hat{\alpha}_i^* + \ln(1 - \beta_i))^2] \\ &= \int_0^1 ((H_n - H_{n-r_i}) + \ln(1 - \beta_i))^2 dP(\beta_i) \\ &= \underbrace{\int_0^1 \ln(1 - \beta_i)^2 dP(\beta_i)}_A - (H_n - H_{n-r_i})^2 \end{aligned}$$

where  $dP(\beta_i)$  is taken to mean integration with respect to the measure induced by  $\beta_i \sim \text{Beta}(i, n + 1 - r_i)$ . Focusing on the remaining integral, we have the closed form:

$$A = (H_n - H_{n-r_i})^2 + \psi'(n + 1 - i) - \psi'(n + 1),$$

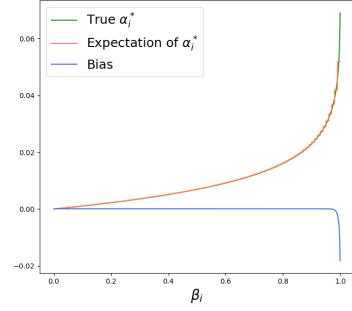


**Figure 1:** Bias of the weights as a function of  $\beta_i$  for  $n = 100$ .

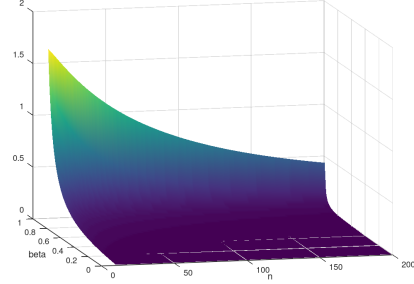


**Figure 2:** The upper bound in Eq. (23) as a function of  $n$  and  $\beta_i$ .

and the result:

$$\text{MSE}(n\hat{\alpha}_i^*) = \psi'(n + 1 - i) - \psi'(n + 1).$$

This term involves the first derivative of the digamma function for which the inequality  $\frac{1}{n} + \frac{1}{2n^2} \leq \psi'(n) \leq \frac{1}{n} + \frac{1}{n^2}$  is well known. Applying these inequalities, we obtain

$$\begin{aligned} \text{MSE}(n\hat{\alpha}_i^*) &\leq \frac{1}{n + 1 - r_i} + \frac{1}{(n + 1 - r_i)^2} - \frac{1}{n + 1} - \frac{1/2}{(n + 1)^2} \\ &= \mathcal{O}\left(\frac{1}{n - r_i + 1} - \frac{1}{n + 1}\right) = \mathcal{O}\left(\frac{\beta_i}{n(1 - \beta_i) + 1}\right) \end{aligned}$$

By analogous reasoning determining a lower bound on the MSE, we achieve the result

$$\text{MSE}(n\hat{\alpha}_i^*) \asymp \frac{\beta_i}{n(1 - \beta_i) + 1} \quad \forall \beta_i \in (0, 1). \quad (23)$$

Then since

$$\begin{aligned} \frac{1}{n} \sum_{i=1}^n \text{MSE}(n\hat{\alpha}_i^*) &\rightarrow \int_0^1 \frac{\beta}{n(1 - \beta) + 1} d\beta \\ &= \frac{(n + 1) \ln(n + 1)}{n^2} - \frac{1}{n} \\ &= \mathcal{O}\left(\frac{\ln(n)}{n}\right) \end{aligned} \quad (24)$$

we have

$$\text{MSE}\left(\sum_{i=1}^n \hat{\alpha}_i^*\right) = \frac{1}{n^2} \sum_{i=1}^n \text{MSE}(n\hat{\alpha}_i^*) = \mathcal{O}\left(\frac{\ln(n)}{n^2}\right) \quad (25)$$

which concludes our proof.  $\square$

## 4 EXPERIMENTS

**Datasets.** We use images datasets such as CIFAR-10/100 (Krizhevsky et al., 2009) and ImageNet (Deng et al., 2009), and a text dataset i.e Amazon Reviews (Ni et al., 2019). The Amazon dataset contains review text inputs paired with 1-out-of-5 star ratings as labels.

**Models.** For experiments on CIFAR10/100, we report the results on the VGG (Simonyan and Zisserman, 2014) models with batch norm layers, WideResNet28x10 (Zagoruyko, 2016), and ResNet (He et al., 2016) models with different depths (20, 56, 110, 164). For each model architecture, we have 5 different models that are pre-trained on the CIFAR10/100 dataset. For experiments on Amazon dataset, we use pre-trained transformer-based models – BERT (Devlin, 2018), RoBERTa (Liu et al., 2021a), Distill-Bert (Sanh, 2019) (D-BERT), and Distill-Roberta (D-RoBERTa)<sup>2</sup>. For experiments on the ImageNet dataset, we use the pre-trained models from *timm* (Wightman, 2019) package, including two vision transformer (ViT) (Dosovitskiy, 2020) variants, ViT-Small and ViT-Large; and two Swin transformer-based models (Liu et al., 2021b), Swin-Base and Swin-Tiny. All these models are configured with standard image resolution – 224.

**Metrics.** For our comparative analysis, we evaluate several metrics including our Monte Carlo plug-in estimator in Eq. (19), the population  $AURC_a$  and the population  $AURC_p$ , alongside the SELE score (Franc et al., 2023). The  $AURC_p$  is calculated via Eq. (5) over the whole test set, while the  $AURC_a$  is computed through the plug-in estimator with weights derived from Eq. (14). Additionally, we consider an approximation of  $AURC_p$  utilizing a 0/1 loss, as detailed in Geifman et al. (2018). We also explore the  $2 \times$ SELE, posited as an upper bound for  $AURC_p$  by Franc et al. (2023), in contrast to the SELE score, which serves as a lower bound for  $AURC_p$ . Beyond the 0/1 loss, we incorporate the metrics with the Cross-Entropy (CE) loss that serves as a complementary measure for assessing the classifier’s performance.

**Experimental setup.** We evaluate the metrics using several pre-trained models on the test set, which is randomly divided into various batch sizes (8, 16, 32,  $\dots$ , 1024). We use MSP as our confidence score function, compute the metrics for these batch samples, and subsequently calculate the mean and

standard deviation of these finite sample estimators. The population  $AURC_p$  is computed across all samples in the whole test set. For the CIFAR10/100 datasets, we evaluate the mean and standard deviation of the Mean Absolute Error (MAE) across five distinct pre-trained models. To facilitate an equitable comparison among the estimators, we compute the MAE based on the  $AURC_p$  rather than  $AURC_a$ . For the ImageNet and Amazon datasets, we compute the mean, standard deviation, and MSE for different estimators of the pre-trained model across batch samples.

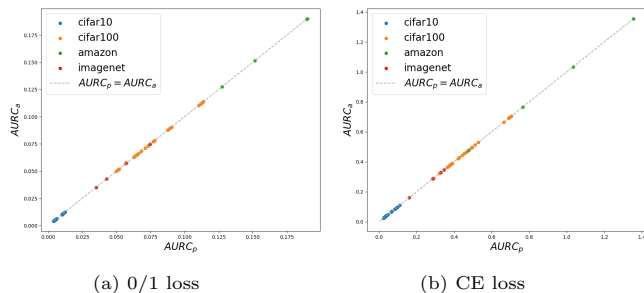
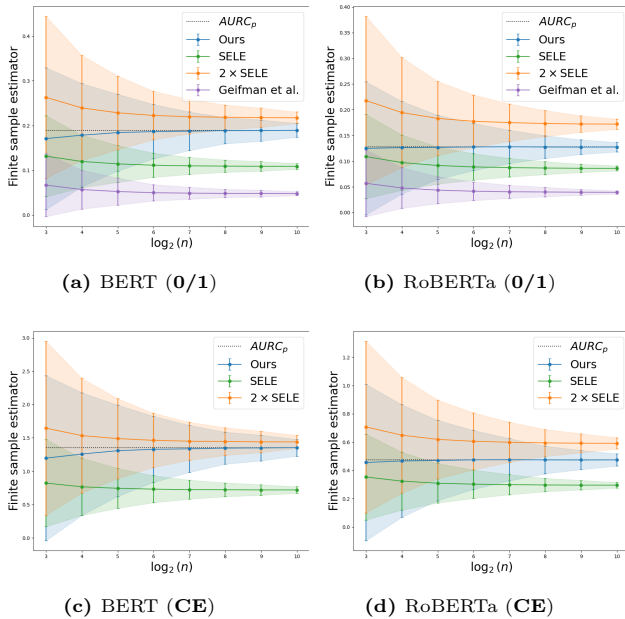


Figure 3: Plot of  $AURC_a$  versus  $AURC_p$

**Comparison between of  $AURC_a$  and  $AURC_p$ .** We evaluate the two population AURC metrics using either 0/1 or CE loss across 30 different models on test sets from CIFAR10/100. Additionally, we assess the previously mentioned models on the test sets from Amazon and ImageNet datasets. The results are reported in Figure 3, where these two population AURC metrics appear almost identical to each other. We also assessed the results using a two-sided t-test, which yielded p-values of 0.9981 and 0.998 for the 0/1 and CE loss, respectively. These values suggest that we should accept the null hypothesis that these two metrics are identical. For convenience, subsequent sections will report only the results for  $AURC_p$ .

**Measure the statistical properties of the estimators.** From Figure 4, it is observable that with 0/1 loss (accuracy) and increasing sample size, both the SELE score and Geifman’s approximation tend to underestimate the population  $AURC_p$ . Conversely,  $2 \times$  SELE consistently overestimates the population  $AURC_p$ , acting as an upper bound. As the sample size grows, our proposed estimator progressively converges to the population  $AURC_p$ . Similar trends can also be observed regardless of the 0/1 loss or CE loss in Figure S7-S12. Furthermore, a comparison between Figure 4(a) and 4(c) reveals that using CE loss rather than 0/1 loss results in higher variance and bias in the estimators. The bias plots in Figure S1-S4 show similar findings. In Figure 5, the MAE of our estimator consistently diminishes as the sample size increases across various pre-trained models. Conversely,

<sup>2</sup>Obtained from RoBERTa with the same procedure as Sanh (2019)



**Figure 4: (Amazon)** Finite sample estimators with 0/1 or CE loss. We utilize a pre-trained model and randomly divide the test set into batch samples of size  $n$ . Subsequently, we compute the mean and std of various estimators applied to these batch samples.

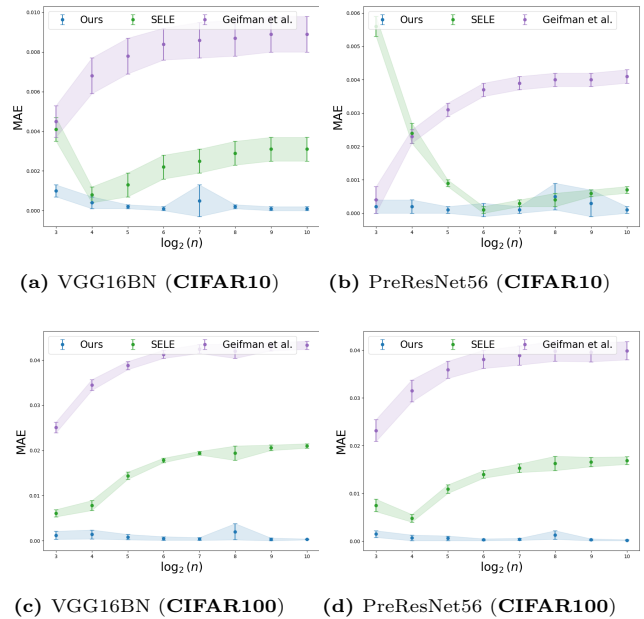


**Figure 5: (CIFAR10/100)** MAE of different finite sample estimators evaluated with 0/1 loss. For each model architecture, we compute the mean and std of the MAE across five distinct pre-trained models. The MAE for each model is calculated using batch samples divided from the test set.

the MAE of Geifman’s approximation tends to increase with the sample size. For the SELE score, when combining with the 0/1 loss, it exhibits an MAE comparable to our estimator when applied to models such as PreResNet56 on the CIFAR10 dataset, as indicated in Figure 5(b). However, as demonstrated in Figure 5(c) and 5(d), its performance lacks stability compared with our approach. Its performance can be even worse on the CIFAR100 dataset when given a large sample size. Results shown in Figure 6 also indicate a declining trend in the MSE of our estimator for the ImageNet dataset as the sample size increases, regardless of whether 0/1 or CE loss is used. Similar MSE results are also observed across other model architectures for the CIFAR10/100 and Amazon datasets (see Figure S13-S18).

**Influence of the CSFs.** We also examine the impact of various CSFs on the estimators to provide a thorough evaluation of the metrics. Specifically, we consider MSP, Negative Entropy, MaxLogit, Softmax Margin, MaxLogit- $\ell_2$  norm, and Negative Gini Score, as outlined in Table S1. The sample size is set to 128. We report the results for Amazon and ImageNet datasets as shown in Figure S19-S21. As indicated in Figure 7, our finite sample estimator exhibits lower bias compared to other estimators across various CSFs. The  $2 \times \text{SELE}$  score does not always act as an upper bound for  $\text{AURC}_p$  especially when Negative

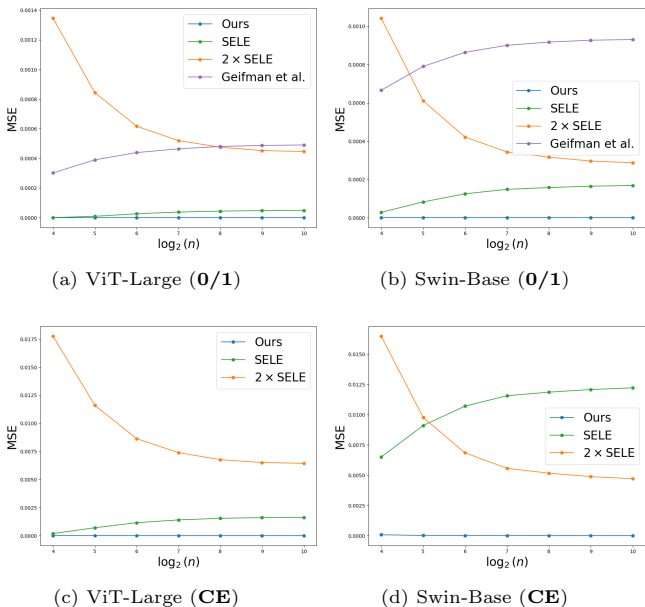


**Figure 6: (ImageNet)** MSE of finite sample estimators with 0/1 or CE loss.

Entropy, MaxLogit- $\ell_2$  norm, and Negative Gini Score are utilized as CSFs. Furthermore, the SELE score and Geifman’s approximation consistently underestimate the population  $\text{AURC}_p$  across various CSFs in

**Table 1:**  $AURC_p(10^{-2})$  of the test set of models that are fine-tuned with different loss functions on the training set. The mean and standard deviation of the  $AURC_p$  is computed across five distinct models that are fine-tuned with different seeds from the same pre-trained model.

Model	CIFAR10			CIFAR100		
	Ours	CE	SELE	Ours	CE	SELE
ResNet18	<b>5.28</b> $\pm$ 0.024	7.24 $\pm$ 0.209	7.11 $\pm$ 0.225	<b>6.29</b> $\pm$ 0.004	6.45 $\pm$ 0.012	6.47 $\pm$ 0.016
ResNet34	<b>6.06</b> $\pm$ 0.121	8.78 $\pm$ 0.165	8.66 $\pm$ 0.149	<b>5.71</b> $\pm$ 0.012	5.90 $\pm$ 0.028	5.94 $\pm$ 0.031
ResNet50	<b>9.84</b> $\pm$ 0.156	13.67 $\pm$ 0.265	13.54 $\pm$ 0.403	<b>5.96</b> $\pm$ 0.017	6.22 $\pm$ 0.028	6.26 $\pm$ 0.032
VGG16BN	<b>5.63</b> $\pm$ 0.069	7.44 $\pm$ 0.300	7.34 $\pm$ 0.299	<b>8.13</b> $\pm$ 0.019	8.64 $\pm$ 0.076	8.64 $\pm$ 0.068
VGG19BN	<b>6.36</b> $\pm$ 0.071	8.29 $\pm$ 0.291	8.24 $\pm$ 0.312	<b>8.18</b> $\pm$ 0.022	8.63 $\pm$ 0.077	8.60 $\pm$ 0.081
WideResNet28x10	<b>3.86</b> $\pm$ 0.129	4.41 $\pm$ 0.207	4.33 $\pm$ 0.183	<b>5.01</b> $\pm$ 0.088	5.08 $\pm$ 0.108	5.09 $\pm$ 0.106

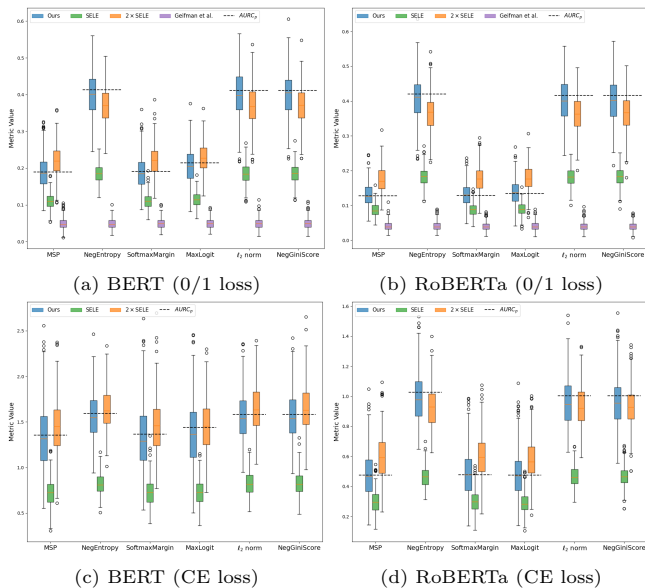


**Figure 7:** (Amazon) Finite sample estimators with different CSFs.

our evaluations. We can also observe that compared to CSFs, both  $AURC_p$  and its finite sample estimators are more sensitive to the choice of loss functions. When using 0/1 loss, they display higher variance than CE loss. For Negative Entropy, MaxLogit- $\ell_2$  norm, and Negative Gini Score, these CSFs exhibit similar impacts on the finite sample estimators. Similar findings can also be observed from Figure S20-S21.

**Training a selective classifier.** We can fine-tune our pre-trained model using these finite sample estimators as a loss function. The MSP is employed as the CSF when evaluating the metrics. The models in Table 1 are fine-tuned on the training set using our Monte Carlo estimator in Eq. (19) along with CE loss as the loss function for the training batches over 30 epochs, using a learning rate of  $10^{-3}$ . We set the training batch size to be 128. Additionally, we present the results for

both CE loss and SELE score, as detailed in Table 1 for the CIFAR10/100 dataset. The population  $AURC_p$  is computed across all the samples within the test set. As indicated by Table 1, training with the Monte Carlo estimator can effectively optimize the  $AURC_p$  compared with the SELE score. Moreover, while training with SELE loss accelerates the optimization of  $AURC_p$  more effectively than CE loss, it remains less effective compared to our estimator.

## 5 CONCLUSION

In this work, we revisit the definition of population AURC and give an asymptotic expression for it, which can be interpreted as a reweighted risk function. Subsequently, we introduce a plug-in estimator for this asymptotic expression, characterized by a biased weight estimator. In the presence of the correlation between CSFs and the loss function, while we are not able to provide theoretical results for this plug-in estimator, we can analyze the bias and MSE of the weight estimator. We demonstrate the effectiveness of our estimator across various state-of-the-art neural network models and several widely-used datasets. Notably, our estimator exhibits lower bias relative to other estimators, especially when the sample size is large, thus providing a more accurate estimate of the population AURC.

## Acknowledgement

This research received funding from the Flemish Government (AI Research Program) and the Research Foundation - Flanders (FWO) through project number G0G2921N. HZ is supported by the China Scholarship Council.

## References

- Abdar, M., Pourpanah, F., Hussain, S., Rezazadegan, D., Liu, L., Ghavamzadeh, M., Fieguth, P., Cao, X., Khosravi, A., Acharya, U. R., et al. (2021). A review of uncertainty quantification in deep learning: Techniques, applications and challenges. *Information fusion*, 76:243–297.
- Belghazi, M. I. and Lopez-Paz, D. (2021). What classifiers know what they don’t? *arXiv preprint arXiv:2107.06217*.
- Berk, R., Heidari, H., Jabbari, S., Kearns, M., and Roth, A. (2021). Fairness in criminal justice risk assessments: The state of the art. *Sociological Methods & Research*, 50(1):3–44.
- Cattelan, L. F. P. and Silva, D. (2023a). How to fix a broken confidence estimator: Evaluating post-hoc methods for selective classification with deep neural networks. *arXiv preprint arXiv:2305.15508*.
- Cattelan, L. F. P. and Silva, D. (2023b). On selective classification under distribution shift. In *NeurIPS 2023 Workshop on Distribution Shifts: New Frontiers with Foundation Models*.
- Chow, C. (1970). On optimum recognition error and reject tradeoff. *IEEE Transactions on information theory*, 16(1):41–46.
- Deng, J., Dong, W., Socher, R., Li, L.-J., Li, K., and Fei-Fei, L. (2009). Imagenet: A large-scale hierarchical image database. In *2009 IEEE conference on computer vision and pattern recognition*, pages 248–255. Ieee.
- Devlin, J. (2018). Bert: Pre-training of deep bidirectional transformers for language understanding. *arXiv preprint arXiv:1810.04805*.
- Dosovitskiy, A. (2020). An image is worth 16x16 words: Transformers for image recognition at scale. *arXiv preprint arXiv:2010.11929*.
- Dvijotham, K., Winkens, J., Barsbey, M., Ghaisas, S., Stanforth, R., Pawlowski, N., Strachan, P., Ahmed, Z., Azizi, S., Bachrach, Y., et al. (2023). Enhancing the reliability and accuracy of ai-enabled diagnosis via complementarity-driven deferral to clinicians. *Nature Medicine*, 29(7):1814–1820.
- El-Yaniv, R. et al. (2010). On the foundations of noise-free selective classification. *Journal of Machine Learning Research*, 11(5).
- Franc, V., Prusa, D., and Voracek, V. (2023). Optimal strategies for reject option classifiers. *Journal of Machine Learning Research*, 24(11):1–49.
- Gal, Y. and Ghahramani, Z. (2016). Dropout as a bayesian approximation: Representing model uncertainty in deep learning. In *international conference on machine learning*, pages 1050–1059. PMLR.
- Geifman, Y., Uziel, G., and El-Yaniv, R. (2018). Bias-reduced uncertainty estimation for deep neural classifiers. *arXiv preprint arXiv:1805.08206*.
- Gomes, E. D. C., Romanelli, M., Granese, F., and Piantanida, P. (2022). A simple training-free method for rejection option.
- Groh, M., Badri, O., Daneshjou, R., Koochek, A., Harris, C., Soenksen, L. R., Doraiswamy, P. M., and Picard, R. (2024). Deep learning-aided decision support for diagnosis of skin disease across skin tones. *Nature Medicine*, 30(2):573–583.
- He, K., Zhang, X., Ren, S., and Sun, J. (2016). Deep residual learning for image recognition. In *Proceedings of the IEEE conference on computer vision and pattern recognition*, pages 770–778.
- Hendrycks, D., Basart, S., Mazeika, M., Zou, A., Kwon, J., Mostajabi, M., Steinhardt, J., and Song, D. (2019). Scaling out-of-distribution detection for real-world settings. *arXiv preprint arXiv:1911.11132*.
- Hendrycks, D. and Gimpel, K. (2016). A baseline for detecting misclassified and out-of-distribution examples in neural networks. *arXiv preprint arXiv:1610.02136*.
- Hou, B., Liu, Y., Qian, K., Andreas, J., Chang, S., and Zhang, Y. (2023). Decomposing uncertainty for large language models through input clarification ensembling. *arXiv preprint arXiv:2311.08718*.
- Jones, M. (2009). Kumaraswamy’s distribution: A beta-type distribution with some tractability advantages. *Statistical Methodology*, 6(1):70–81.
- Krizhevsky, A., Hinton, G., et al. (2009). Learning multiple layers of features from tiny images.
- Lakshminarayanan, B., Pritzel, A., and Blundell, C. (2017). Simple and scalable predictive uncertainty estimation using deep ensembles. *Advances in neural information processing systems*, 30.
- Leibig, C., Brehmer, M., Bunk, S., Byng, D., Pinker, K., and Umutlu, L. (2022). Combining the strengths of radiologists and ai for breast cancer screening: a retrospective analysis. *The Lancet Digital Health*, 4(7):e507–e519.
- Liu, T., Cheng, J., and Tan, S. (2023). Spectral bayesian uncertainty for image super-resolution. In *Proceedings of the IEEE/CVF Conference on Computer Vision and Pattern Recognition*, pages 18166–18175.
- Liu, W., Wang, X., Owens, J., and Li, Y. (2020). Energy-based out-of-distribution detection. *Advances in neural information processing systems*, 33:21464–21475.

- Liu, Z., Lin, W., Shi, Y., and Zhao, J. (2021a). A robustly optimized bert pre-training approach with post-training. In *China National Conference on Chinese Computational Linguistics*, pages 471–484. Springer.
- Liu, Z., Lin, Y., Cao, Y., Hu, H., Wei, Y., Zhang, Z., Lin, S., and Guo, B. (2021b). Swin transformer: Hierarchical vision transformer using shifted windows. In *Proceedings of the IEEE/CVF international conference on computer vision*, pages 10012–10022.
- Moon, J., Kim, J., Shin, Y., and Hwang, S. (2020). Confidence-aware learning for deep neural networks. In *international conference on machine learning*, pages 7034–7044. PMLR.
- Ni, J., Li, J., and McAuley, J. (2019). Justifying recommendations using distantly-labeled reviews and fine-grained aspects. In *Proceedings of the 2019 conference on empirical methods in natural language processing and the 9th international joint conference on natural language processing (EMNLP-IJCNLP)*, pages 188–197.
- Sanh, V. (2019). Distilbert, a distilled version of bert: Smaller, faster, cheaper and lighter. *arXiv preprint arXiv:1910.01108*.
- Simonyan, K. and Zisserman, A. (2014). Very deep convolutional networks for large-scale image recognition. *arXiv preprint arXiv:1409.1556*.
- Teye, M., Azizpour, H., and Smith, K. (2018). Bayesian uncertainty estimation for batch normalized deep networks. In *International conference on machine learning*, pages 4907–4916. PMLR.
- Traub, J., Bungert, T. J., Lüth, C. T., Baumgartner, M., Maier-Hein, K. H., Maier-Hein, L., and Jaeger, P. F. (2024). Overcoming common flaws in the evaluation of selective classification systems. *arXiv preprint arXiv:2407.01032*.
- Wei, H., Xie, R., Cheng, H., Feng, L., An, B., and Li, Y. (2022). Mitigating neural network overconfidence with logit normalization. In *International conference on machine learning*, pages 23631–23644. PMLR.
- Wightman, R. (2019). Pytorch image models. <https://github.com/rwightman/pytorch-image-models>.
- Xia, G. and Bouganis, C.-S. (2022). On the usefulness of deep ensemble diversity for out-of-distribution detection. *arXiv preprint arXiv:2207.07517*.
- Xia, G. and Bouganis, C.-S. (2023). Window-based early-exit cascades for uncertainty estimation: When deep ensembles are more efficient than single models. In *Proceedings of the IEEE/CVF International Conference on Computer Vision*, pages 17368–17380.
- Zagoruyko, S. (2016). Wide residual networks. *arXiv preprint arXiv:1605.07146*.
- Zhu, F., Zhang, X.-Y., Cheng, Z., and Liu, C.-L. (2023). Revisiting confidence estimation: Towards reliable failure prediction. *IEEE Transactions on Pattern Analysis and Machine Intelligence*.

## A Appendix

The CSFs are generally defined as functions of the predicted probabilities  $\mathbf{p}_i$ , which are the outputs by passing the logits  $\mathbf{z}$  produced by the model for the input  $x$  through the softmax function  $\sigma(\cdot)$ , expressed as  $\sigma(\mathbf{z}) \in \mathbb{R}^K$ . The specific forms of these CSFs are outlined as follows:

**Table S1:** Commonly Used CSFs

Method	Equation
MSP	$g(\mathbf{z}) = \max_{i=1}^K \mathbf{p}_i$
MaxLogit	$g(\mathbf{z}) = \max_{i=1}^K \mathbf{z}_i$
Softmax Margin	$g(\mathbf{z}) = \mathbf{p}_i - \max_{j \neq i} \mathbf{p}_j$ with $i = \arg \max_{i=1}^K \mathbf{p}_i$
Negative Entropy	$g(\mathbf{z}) = -\sum_{i=1}^K \mathbf{p}_i \log \mathbf{p}_i$
MaxLogit- $\ell_p$ Norm	$g(\mathbf{z}) = \ \mathbf{z}\ _p$
Negative Gini Score	$g(\mathbf{z}) = -1 + \sum_{i=1}^K \mathbf{p}_i^2$

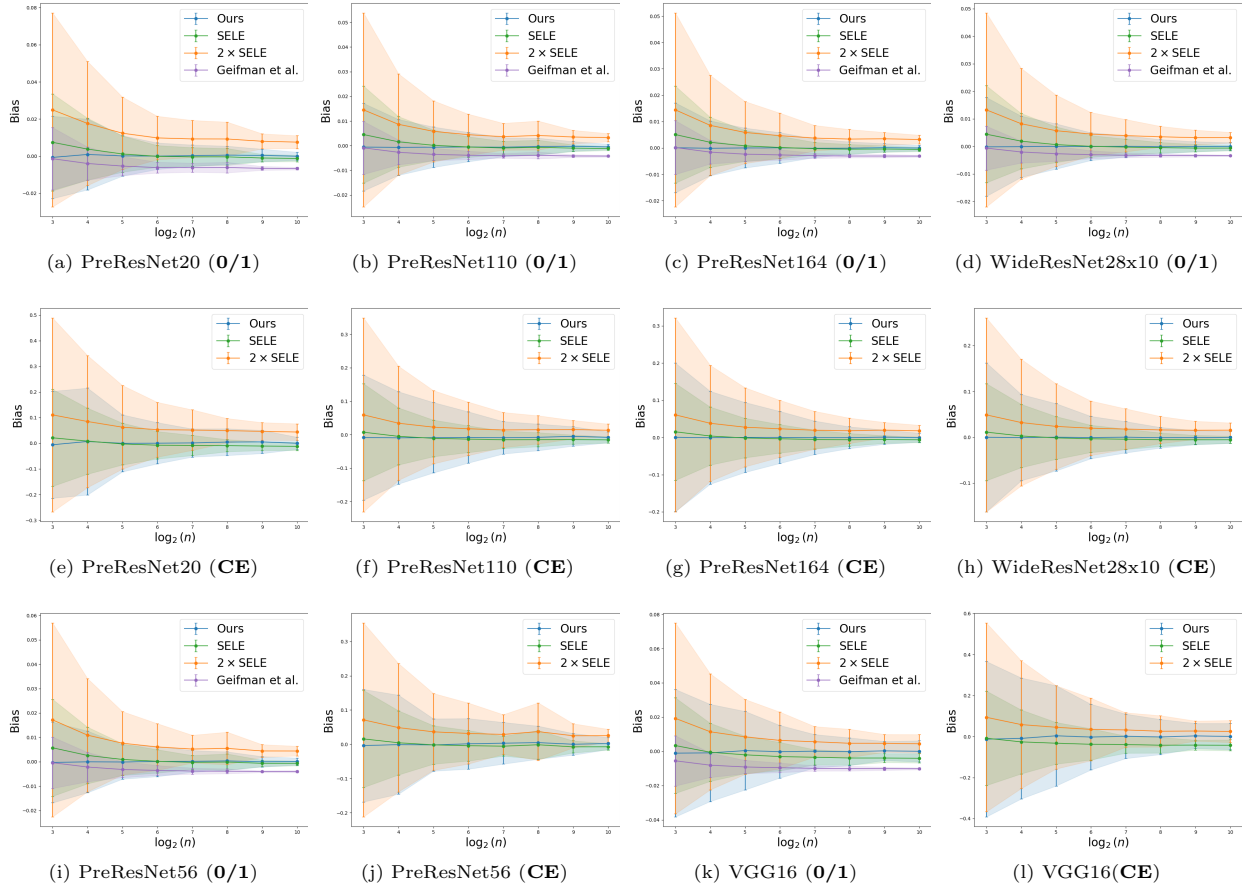


**Figure S1:** (CIFAR10) Bias of different finite sample estimators evaluated with **0/1** or **CE** loss.

## A Novel Characterization of the Population AURC

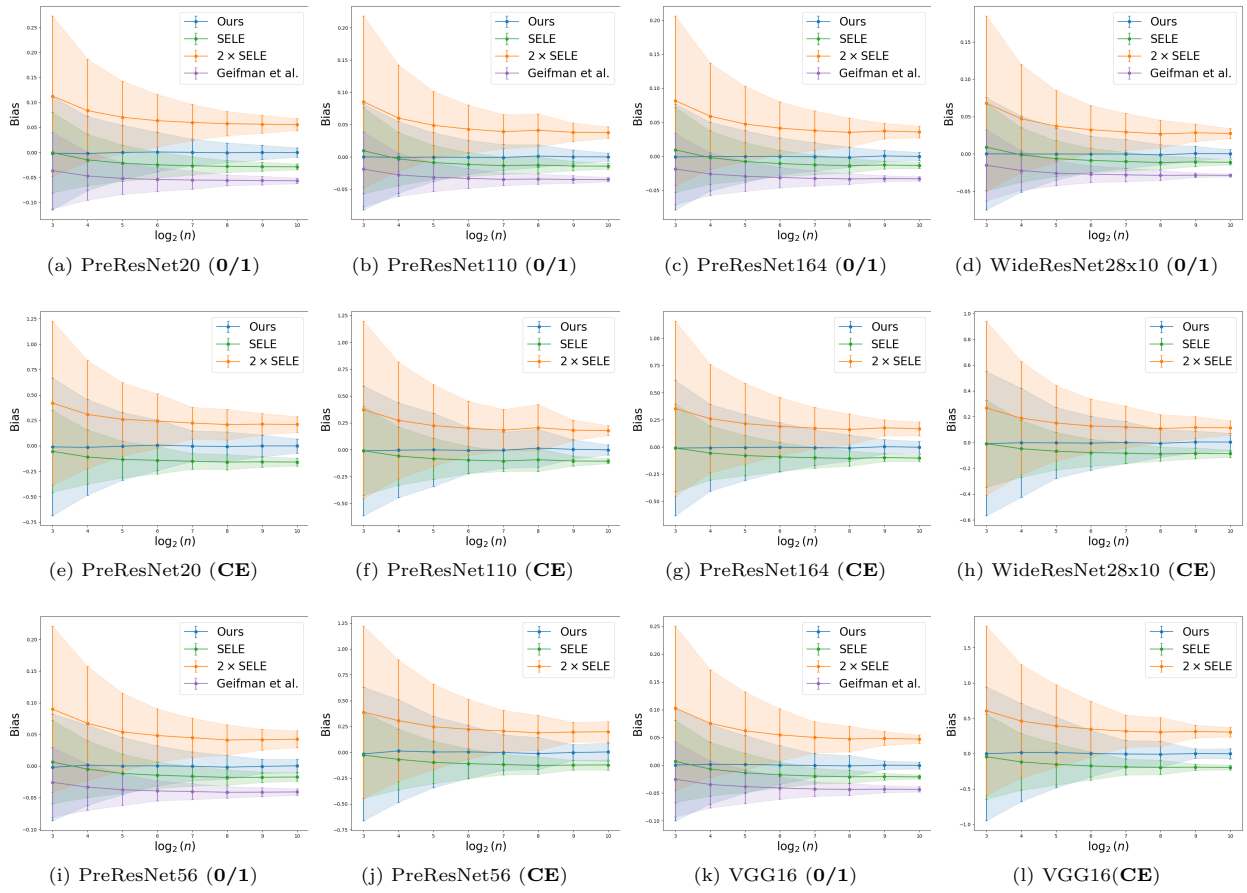


**Figure S2: (CIFAR100) Bias of different finite sample estimators evaluated with 0/1 or CE loss.**

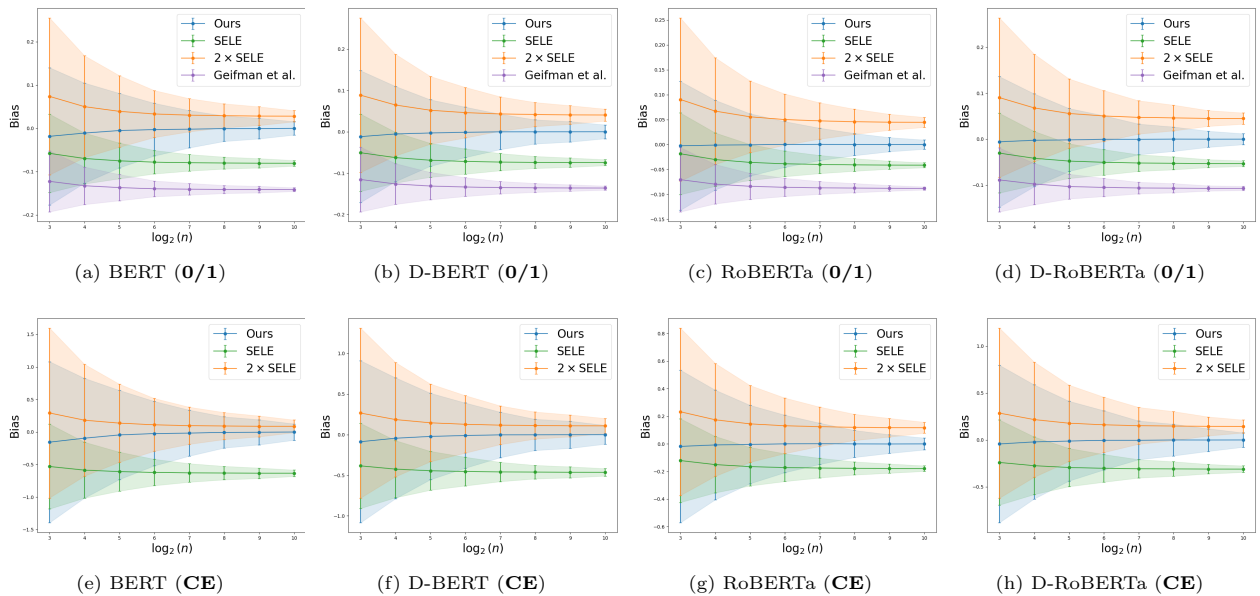


**Figure S3: (Amazon) Bias of different finite sample estimators evaluated with 0/1 or CE loss.**

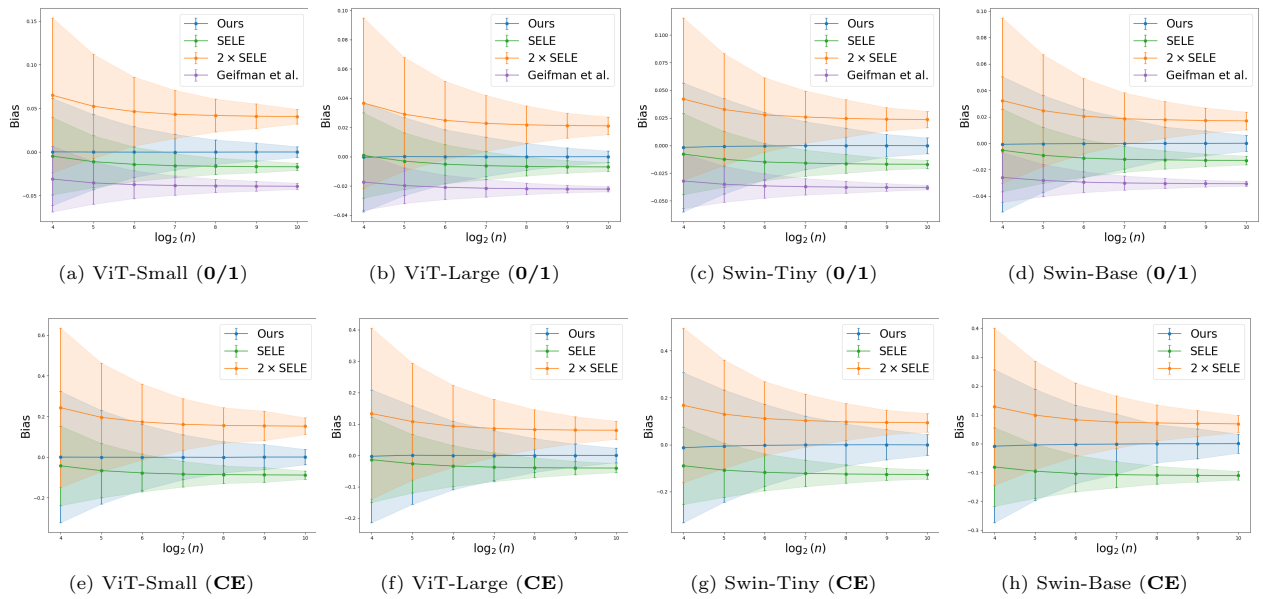


**Figure S4: (ImageNet) Bias of different finite sample estimators evaluated with 0/1 or CE loss.**

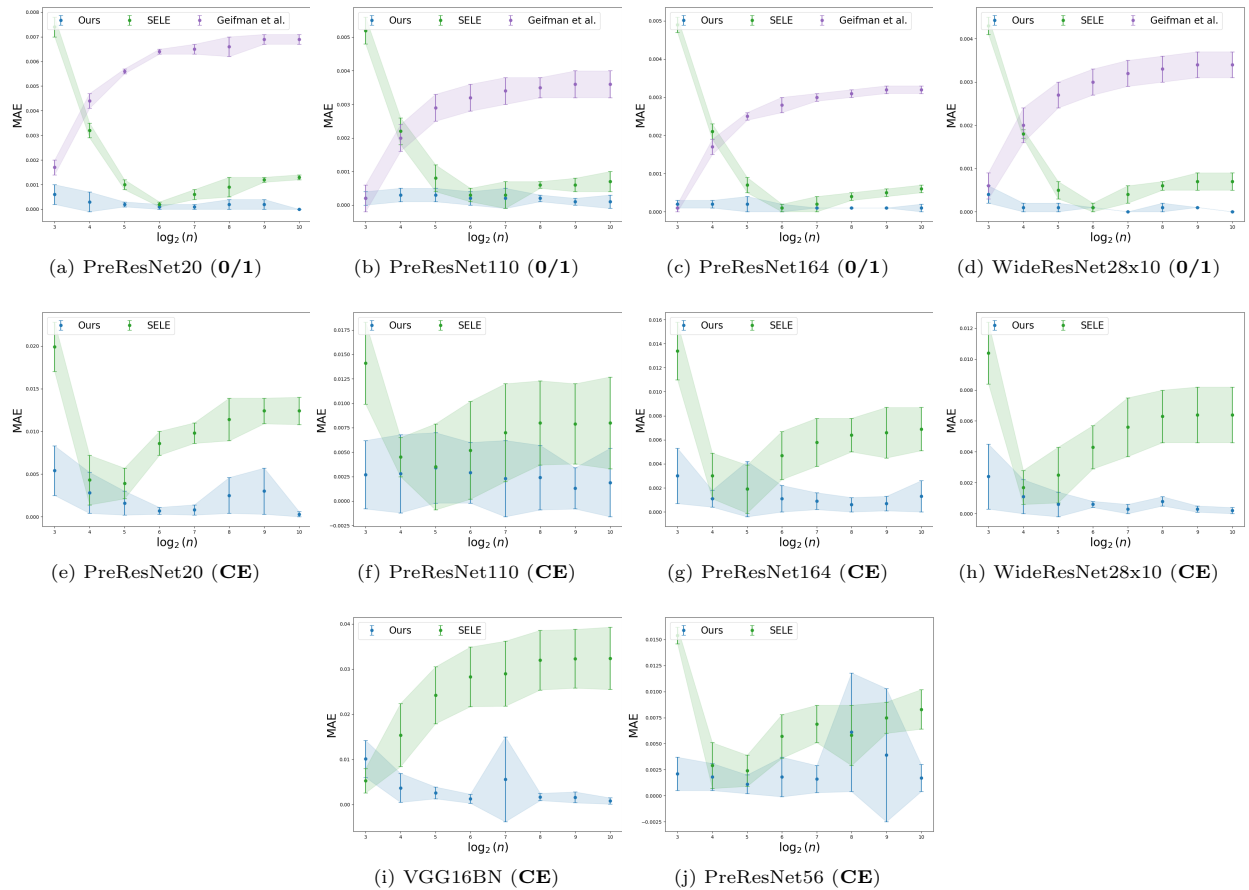


**Figure S5: (CIFAR10) MAE of different finite sample estimators evaluated with 0/1 or CE loss.**

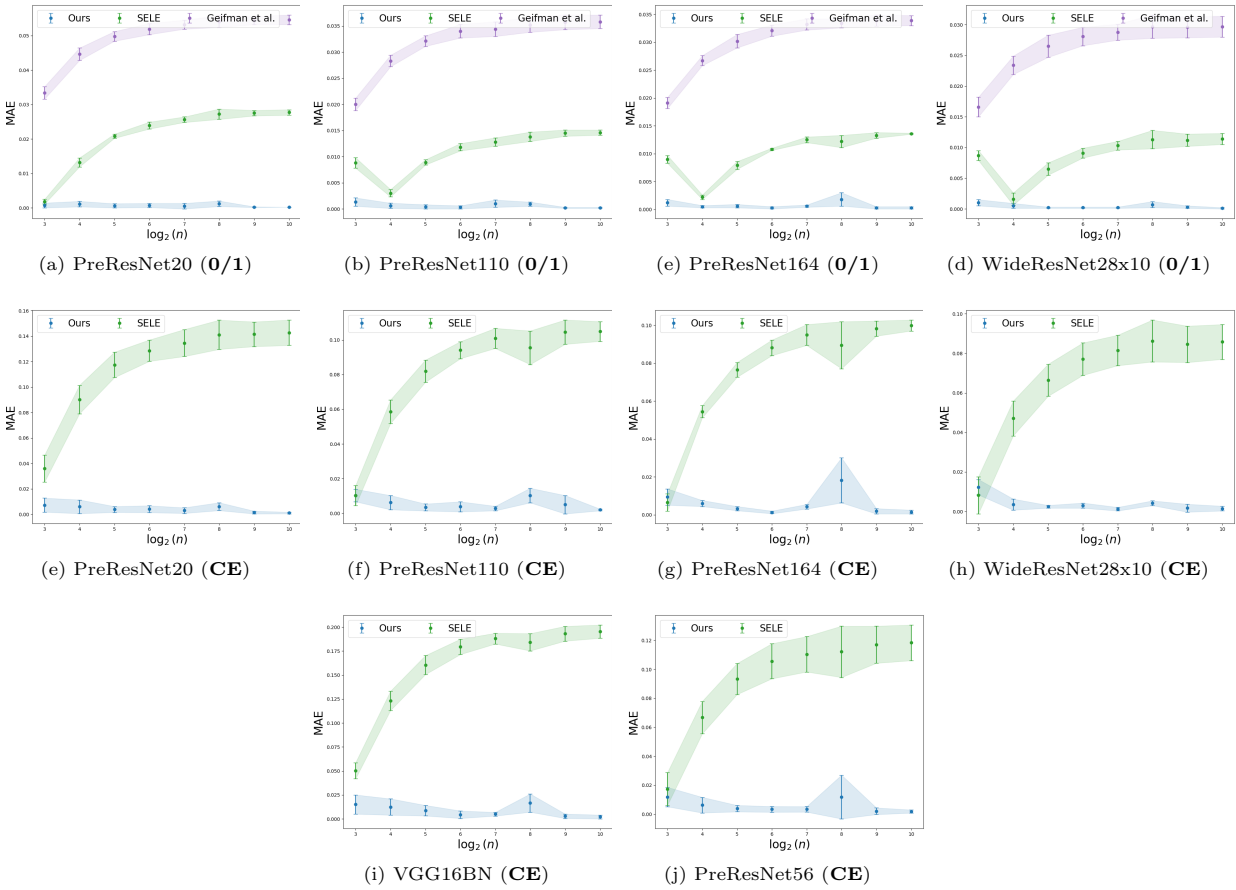


Figure S6: (CIFAR100) MAE of different finite sample estimators evaluated with 0/1 or CE loss.

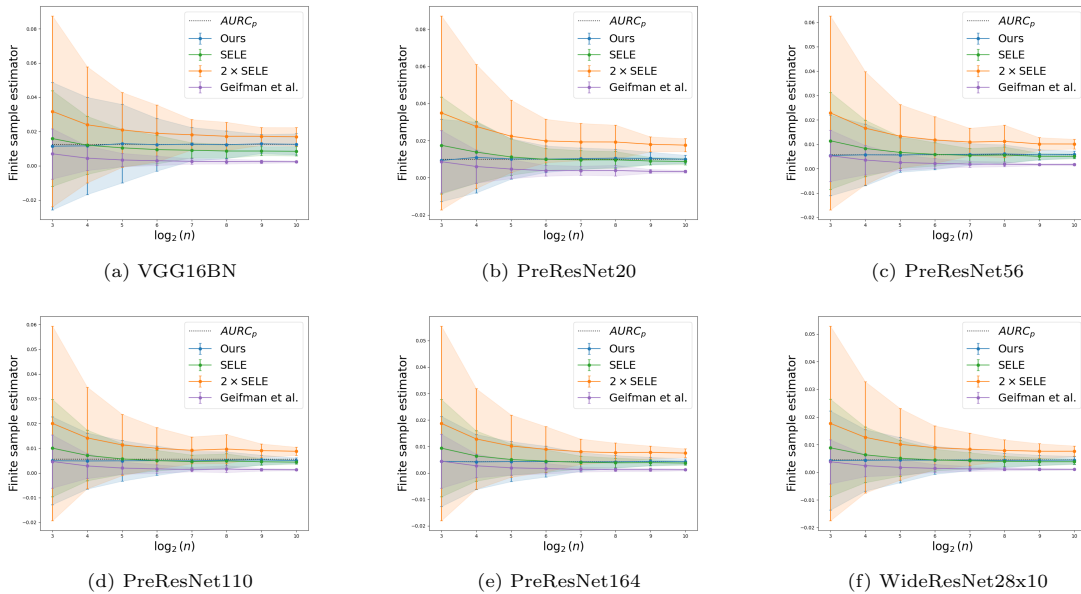
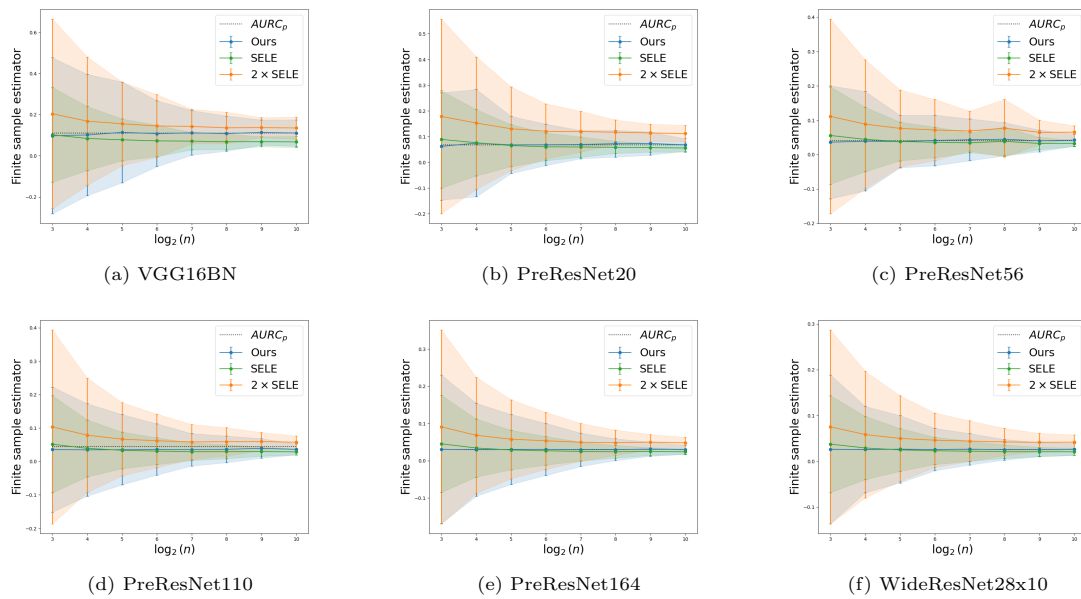
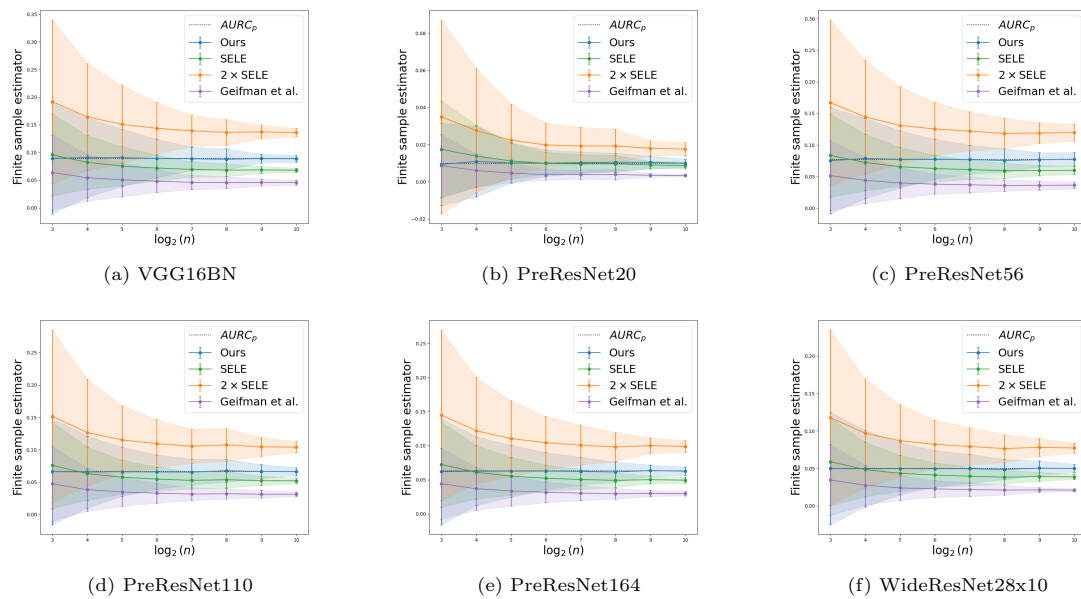


Figure S7: Finite sample estimators on CIFAR10 dataset with 0/1 loss. We utilize a pre-trained model and randomly divide the test set into batch samples of size  $n$ . Subsequently, we compute the mean and variance of various estimators applied to these batch samples. Additionally, the population  $AURC_p$  is computed across all samples in the test set.



**Figure S8:** Finite sample estimators on **CIFAR10** dataset with **CE** loss. The mean and standard deviation are measured using batch samples divided from the test set.



**Figure S9:** Finite sample estimators on the **CIFAR100** dataset with **0/1** loss. The mean and standard deviation are measured using batch samples divided from the test set.

## A Novel Characterization of the Population AURC

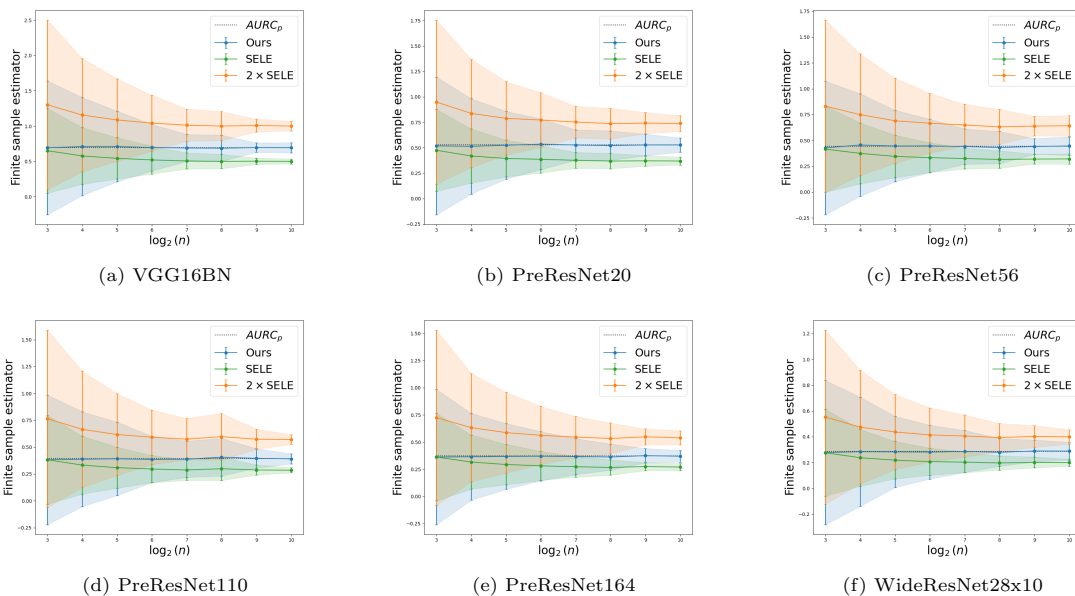


**Figure S10:** Finite sample estimators on the **CIFAR100** dataset with **CE** loss.

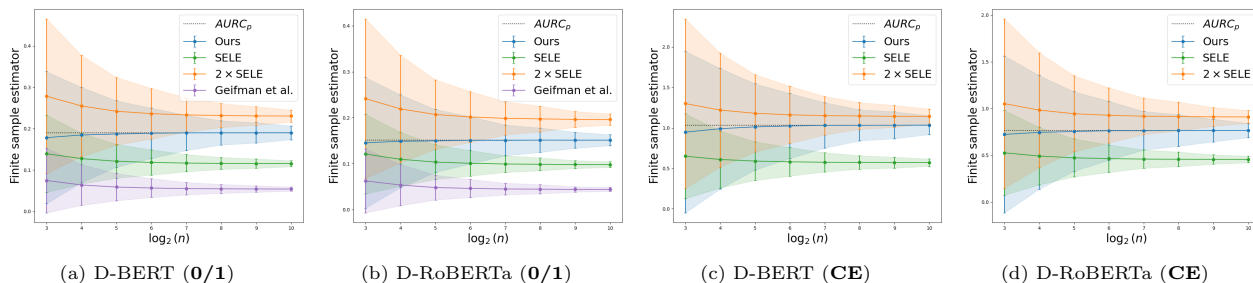


**Figure S11:** (**Amazon**) Finite sample estimators with **0/1** or **CE** loss.

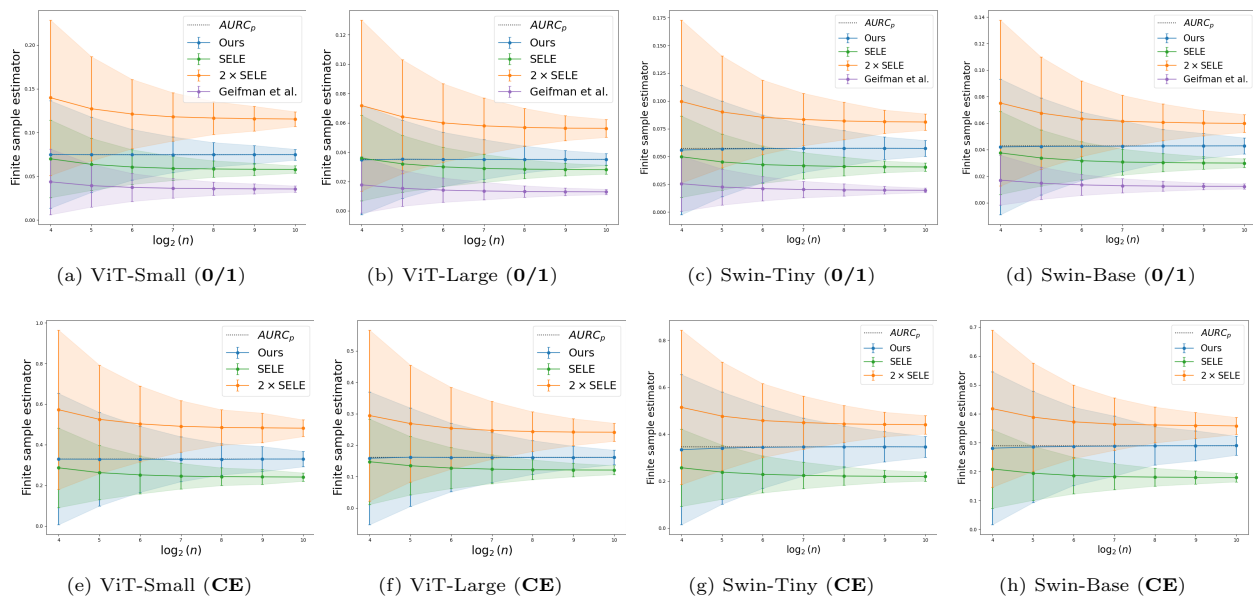


**Figure S12:** (**ImageNet**) Finite sample estimators with **0/1** or **CE** loss. The mean and standard deviation are measured using batch samples divided from the test set.

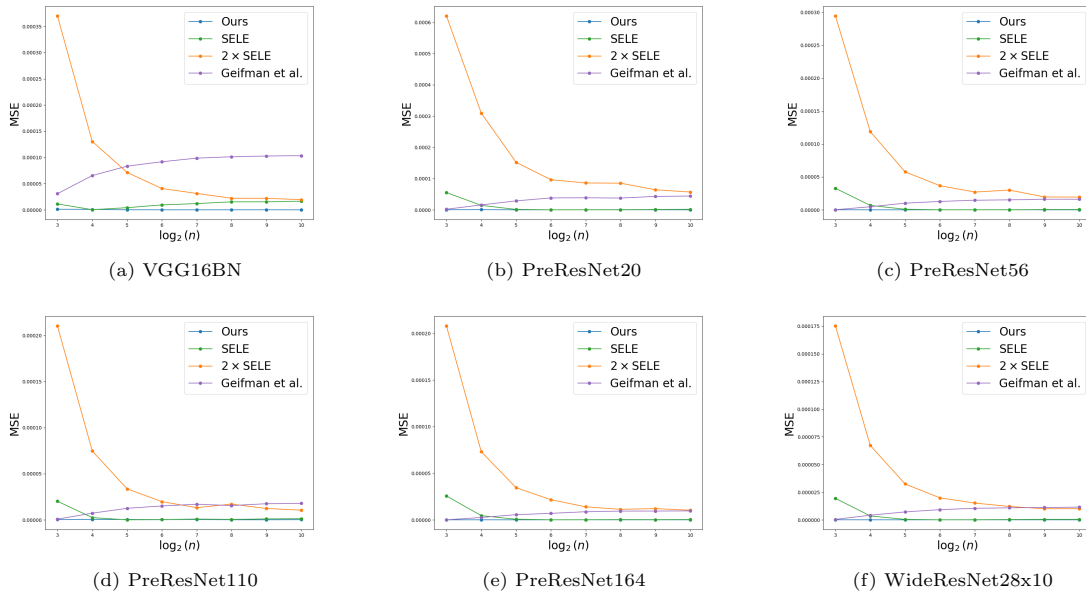


Figure S13: (CIFAR10) MSE of different finite sample estimators with 0/1 loss.

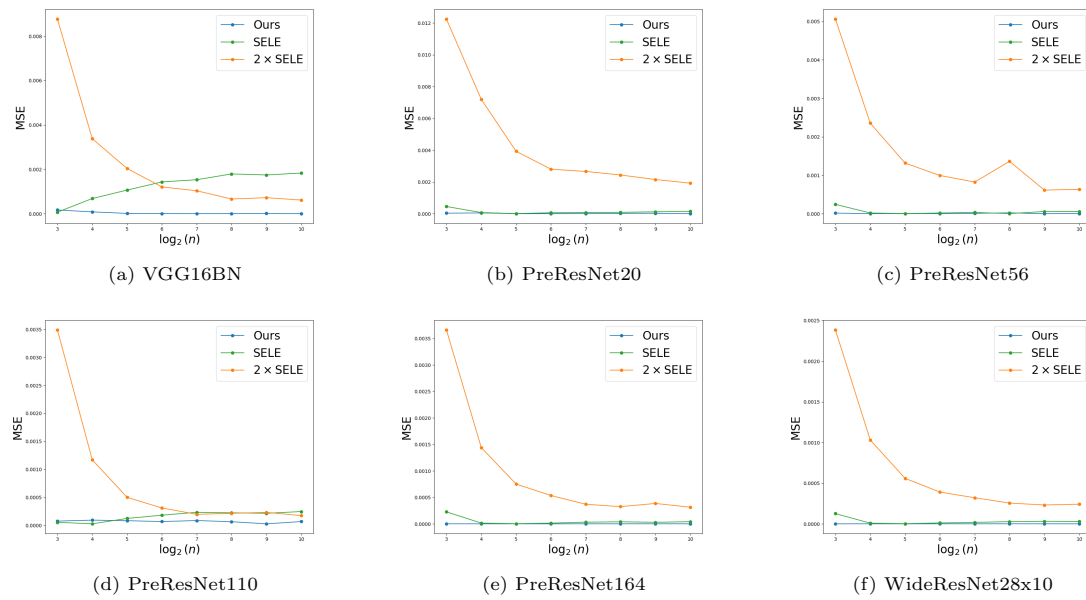
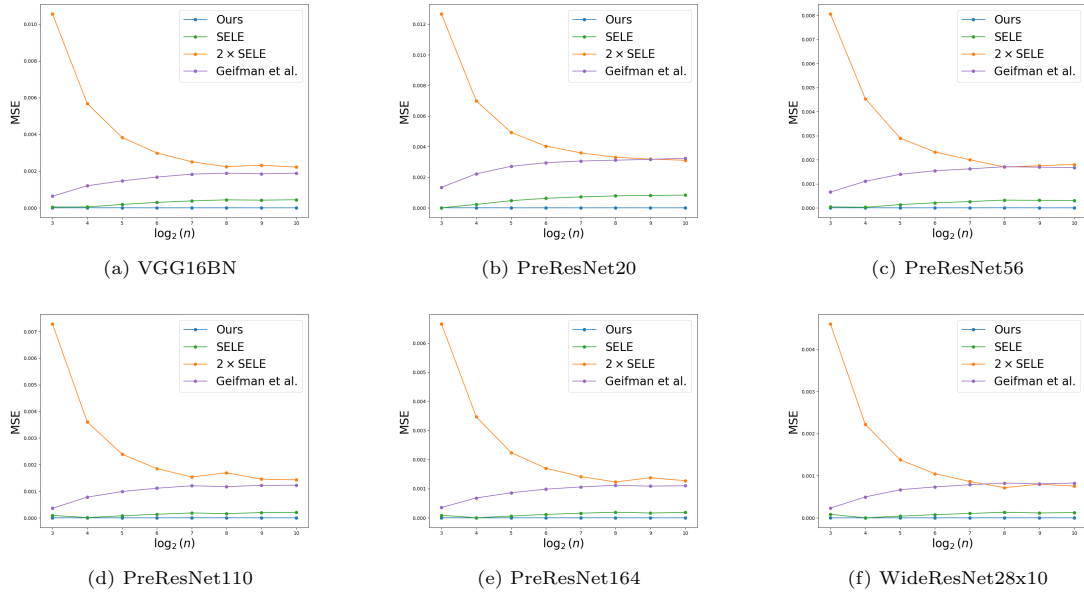
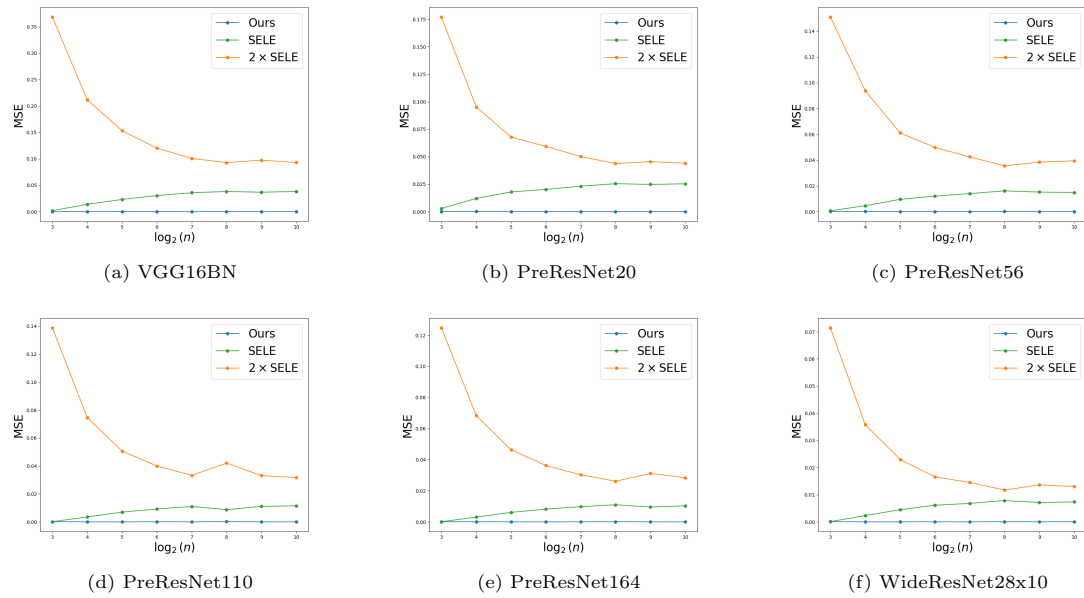


Figure S14: (CIFAR10) MSE of different finite sample estimators with CE loss.

# A Novel Characterization of the Population AURC



**Figure S15: (CIFAR100) MSE of different finite sample estimators with 0/1 loss.**



**Figure S16: (CIFAR100) MSE of different finite sample estimators with CE loss.**

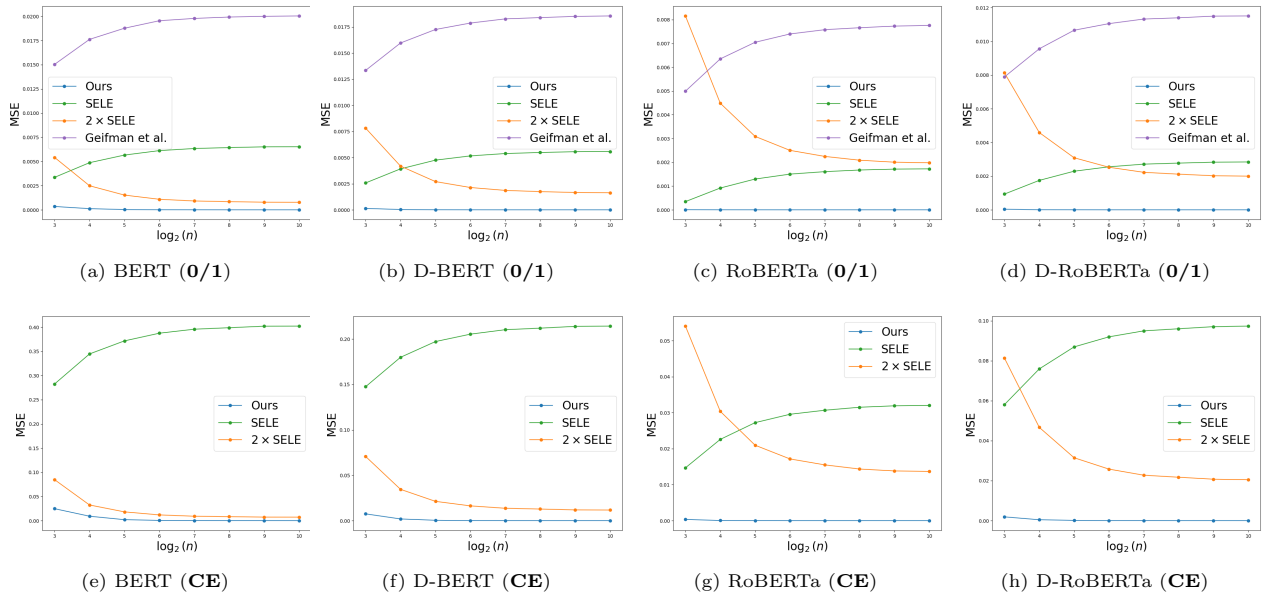


Figure S17: (Amazon) MSE of different finite sample estimators with 0/1 or CE loss.

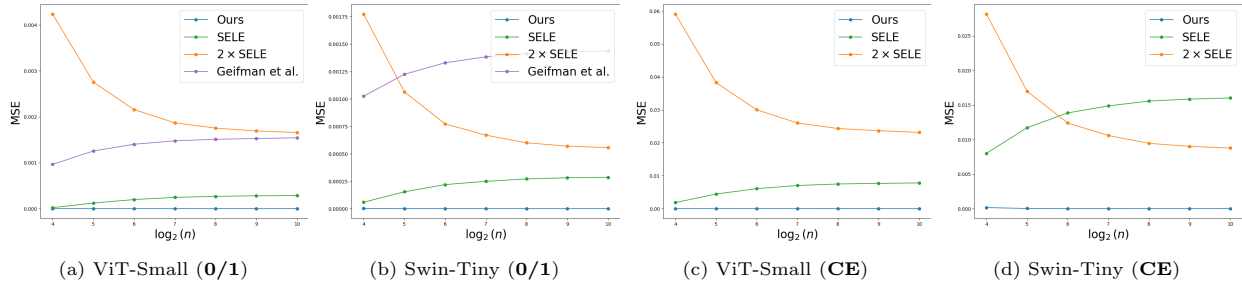


Figure S18: (ImageNet) MSE of finite sample estimators with 0/1 or CE loss.

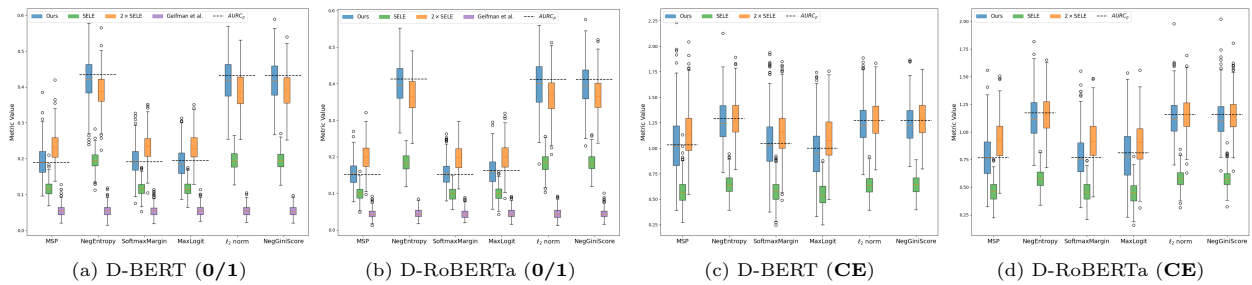


Figure S19: (Amazon) Finite sample estimators that utilize 0/1 or CE loss with different CSFs.

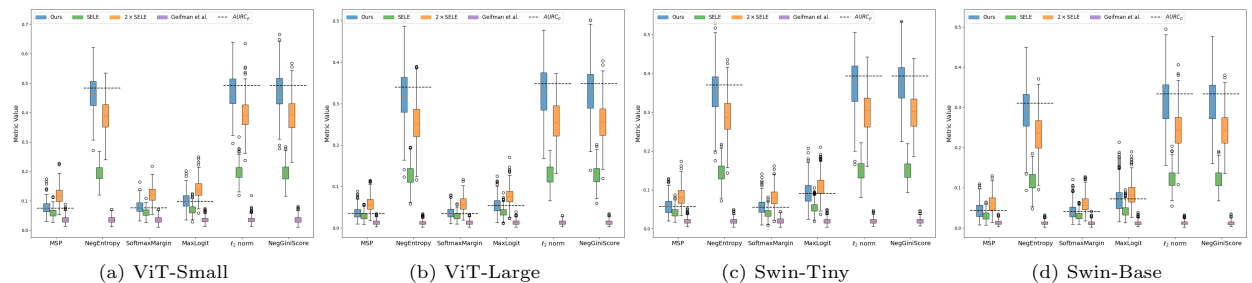


Figure S20: (ImageNet) Finite sample estimators that utilize 0/1 loss with different CSFs.

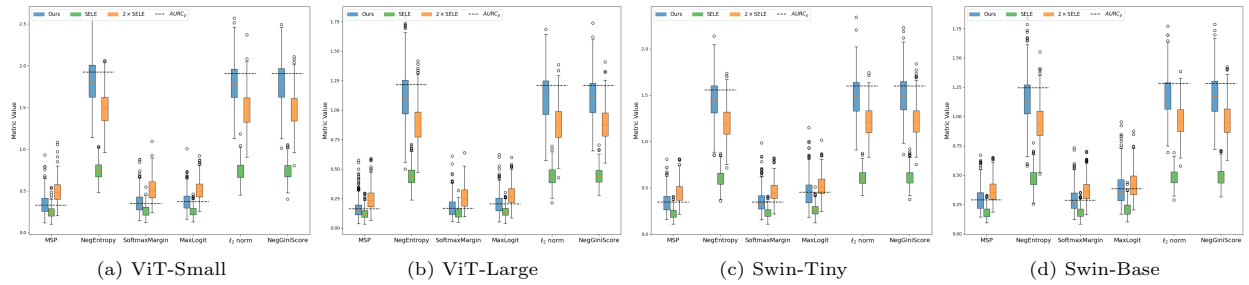


Figure S21: (ImageNet) Finite sample estimators that utilize CE loss with different CSFs.